Supplementary Information

Variants in exons 5 and 6 of *ACTB* cause syndromic thrombocytopenia

Latham *et al.*

Supplementary Note 1

Whole-transcriptome analysis (RNA-Seq)

The global gene expression profile of P4, P5 and healthy control fibroblasts was assessed to evaluate actin isoform transcription and to define a shortlist of affected ABP's, which were subsequently examined at the protein level. RNA was isolated from three independent fibroblast cell culture flasks for each individual and subsequent whole transcriptome sequencing was performed. Principal component analysis shows clear grouping of replicates for each individual and clear separation between samples from different individuals. Gene expression analysis revealed 2307 significantly differentially expressed genes (DEG, Benjamini-Hochberg adjusted P-value ≤ 0.01) when comparing both *ACTB*-AST patients with the healthy control (Supplementary Data 6, see Supplementary Data 4 and Supplementary Data 5 for all DEG identified for each individual). Further conclusions about the impact of these *ACTB* mutations are unable to be drawn from the transcriptome analysis due to the lack of additional healthy control biological replications. Additional studies are needed to assess the impact of *ACTB*-AST mutations on the transcriptome.

In Silico **analysis of mutation-induced structural changes in β-CYA^{P4} and β-CYA^{P5}**

Structural changes in β-CYA^{P4} and β-CYA^{P5} occur in the region of actin SD1 that is formed by residues 338-374. This region is highly conserved in all actin isoforms (Supplementary Fig. 1). The P4 mutation changes 26 amino acids and removes 19 residues (Fig. 6a, left). A deletion of four amino acids in P5 results in a shift of residues G342-S358 by ~5Å, while residues K359-F377 are predicted to be structurally unaffected (Fig. 6a, right).

In both P4 and P5, the binding interfaces for interaction with the CM-loop (T417 – T432) and supporting-loop (E542 – L550) of myosin are affected. The CM-loop is essential for strong binding of myosin's upper 50kDa domain to actin via hydrophobic (NM-2C: V422, V427, A430; β-CYA: V30, P333, Y337) and electrostatic interactions (NM-2C: K429; β-CYA: D25, E334). The absence of C-terminal residues P333, E334 and Y337 in β-CYA^{P4} is predicted to perturb CM-loop binding. A recent cryo-EM structure of the human cytoplasmic actomyosin complex shows that this binding interface is stabilized by internal interactions of W340[1]. This residue interacts with V9, D11 and K18 of the central SD1 β-sheet and forms ring stacking interactions with P27. Our model predicts that absence of W340 in both β-CYA^{P4} and β-CYA^{P5} perturbs the CM-loop binding surface (Fig. 6b, top). This view receives further support from the results of MD-simulations that compare the folding stability and behavior of β-CYA^{WT} and β-CYA^{P5}.

Mutations within the supporting-loop alter the actin-activated ATPase activity, actin affinity and *in vitro* sliding motility of a *Dictyostelium discoideum* myosin 2 motor domain construct[2]. Based on biochemical results, the supporting-loop was reported to interact with actin N-terminal residues[3]. However, this interpretation is not compatible with the structure of a human rigor actomyosin complex that was obtained using electron cryomicroscopy[1]. The structure shows two actin C-terminal glutamines (Q353, Q354) to be within the interaction range of this NM-2 loop. According to our modelling results, these residues are despite the frameshift spatially conserved in β-CYA^{P4}, but out of the interaction range in the case of β-CYA^{P5} (Fig. 6b, bottom).

For the actin-α-actinin complex, a low resolution cryo-EM density is available (PDB: 3LUE, described in [4]), which shows that the binding sites for α-actinin and myosin overlap. The actin binding domain of α-actinin is commonly referred to as calponin homology domain, as it shares its actin binding domain with a large superfamily of proteins including calponin, dystonin, dystrophin, filamin, plectin, and spectrin. The interface includes the interaction of β-CYA SD1 I345 with F101 of α-actinin. For both β-CYA^{P4} and β-CYA^{P5} the hydrophobic interactions of I345 are conserved in the form of leucine residues (Fig. 6c). However, in β-CYA^{P4}, D349 and D351 are within the interaction range of α-actinin H102 and D95, introducing additional electrostatic interactions (Fig. 6c, left).

Regarding α-SMA, despite conservation of C-terminal residues between α-SMA and β-CYA, N-terminal residues are highly divergent (α-SMA: MCEEEDSTAL, β-CYA: MDDDIAAL). These residues are also part of the interaction interfaces of actin with NM-2 (NM2C: R661-R664 within loop2/W-helix) and α-actinin (R93, K96) and may also contribute to the phenotype observed in sub-nuclear bundles.

Transmission Electron Microscopy of *ACTB*-AST platelets

As cytoskeletal defects are associated with compromised platelet ultrastructure[5,6], platelets from healthy control, P3, P4 and P5 were assessed by transmission electron microscopy (Supplementary Figure 10). Our assessment showed that all regular intracellular content in the form of dense granules, α-granules, mitochondria and lysosomes is present in both healthy control and *ACTB*-AST patient platelets. Follow up studies are required for in depth characterization of *ACTB*-AST platelet ultrastructure.

3' *ACTB* variants listed in the gnomAD database

According to ExAC computation[7], *ACTB* is intolerant to both loss-of-function and missense variants. Out of the predicted 188 missense variants, only 12 missense changes are listed in the ExAC database and not a single loss-of-function change (pLI score 0,94; missense z-score 6,29). The number of observed variants increased to 19 in the gnomAD dataset. Of these, 7 are within the 3' region (Supplementary Table 1) and each has only been seen in a single individual. It is not currently known whether these variants listed in the gnomAD database are truly benign, not fully penetrant, or causative for *ACTB*-AST. One variant, p.Glu364Gln, affects the same residue as a mutation described by Nunoi *et al.* (p.Glu364Lys). We expect the patient described by Nunoi *et al.* to have had a stronger clinical phenotype, as the substitution of Glu with Lys is likely to cause more severe consequences on protein structure and function.

β-CYA^{WT}	DRMQKEITAL	APSTMKIKII	A-PPERKYSVW	IGGSILASLS	TFQQMWISKQ	EYDESGPSIV	HRKCF	375
	311	321	331	341	351	361	371	
β-CYA$^{P1/P2}$	DRRQKEITAL	APSTMKIKII	A-PPERKYSVW	IGGSILASLS	TFQQMWISKQ	EYDESGPSIV	HRKCF	375
β-CYA$^{P3/P4}$	DRMQKEITAL	APSTMKIKII	VLRVDRRLHPG	LAVHLPADVD	--QQAGV			357
β-CYA^{P5}	DRMQKEITAL	APSTMKIKII	A-PPERKY---	-GGSILASLS	TFQQMWISKQ	EYDESGPSIV	HRKCF	371
β-CYA^{P6}	DRMQKEITAL	APSTMKIKII	A-PPERKYSVW	IGGSILASLS	TFQQMWISKQ	EYDESGP--L	HRPPQMLLGG L	379
β-CYA^{PN}	DRMQKEITAL	APSTMKIKII	A-PPERKYSVW	IGGSILASLS	TFQQMWISKQ	EYDKSGPSIV	HRKCF	374
γ-CYA	DRMQKEITAL	APSTMKIKII	A-PPERKYSVW	IGGSILASLS	TFQQMWISKQ	EYDESGPSIV	HRKCF	375
α-SMA	DRMQKEITAL	APSTMKIKII	A-PPERKYSVW	IGGSILASLS	TFQQMWISKQ	EYDEAGPSIV	HRKCF	377

Supplementary Figure 1. Schematic representation of *ACTB*-AST mutations. Peptide sequence alignment of wildtype (WT) β-CYA, *ACTB*-AST patient β-CYA, γ-CYA and α-SMA isoforms starting at β-CYA^{WT} residue 311. Residues affected in *ACTB*-AST patients are shown in magenta. The C-terminal residue specific to α-SMA is shown in green.

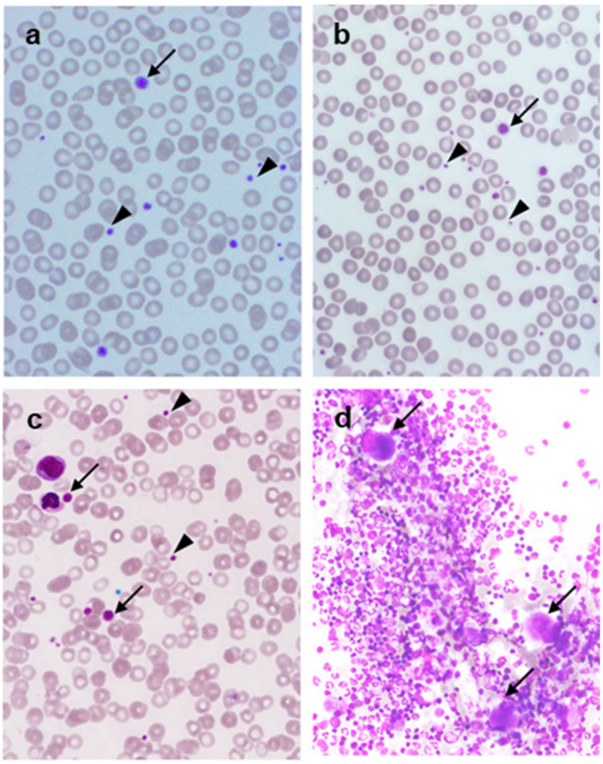

Supplementary Figure 2. Peripheral blood and bone marrow smears of affected individuals. (**a**-**c**) May-Gruenwald-Giemsa-stained stained peripheral blood smears of (**a**) patient 4 (P4), (**b**) patient 3 (P3) and (**c**) patient 5 (P5), with anisocytosis demonstrating normal sized thrombocytes (arrowheads) and macrothrombocytes (arrows); (**d**) May-Gruenwald-Giemsa-stained bone marrow smear of P5 demonstrating numerous megakaryocytes (arrows).

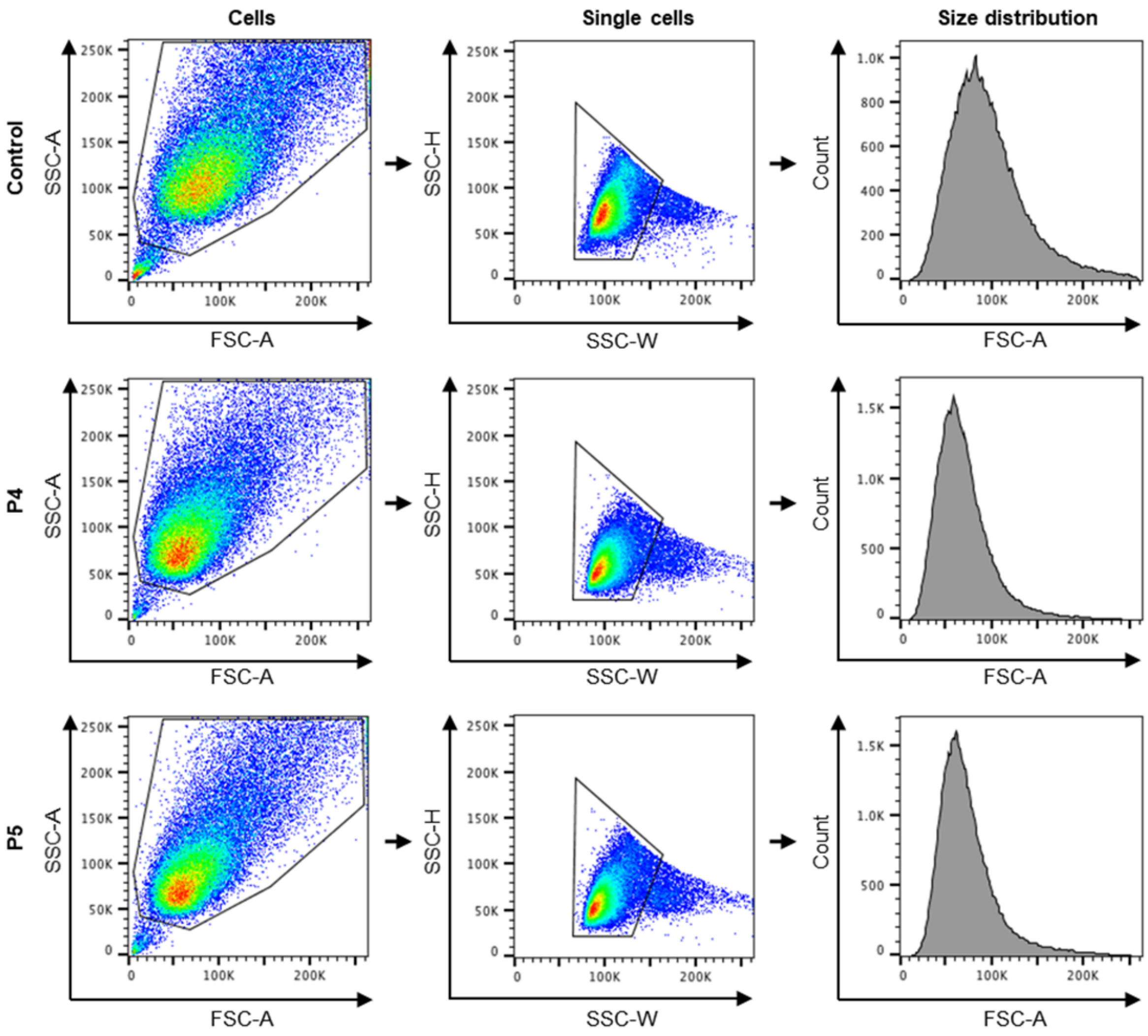

Supplementary Figure 3. Flow cytometry analysis strategy for Fig. 3c. Cells were gated according to forward scatter area (FSC-A) vs side scatter area (SSC-A) and the single cell population was defined by SSC-width vs SSC-height. A frequency histogram was generated for FSC-A, showing a FSC-A left shift for patient 4 (P4) and patient 5 (P5) cells compared to the healthy control.

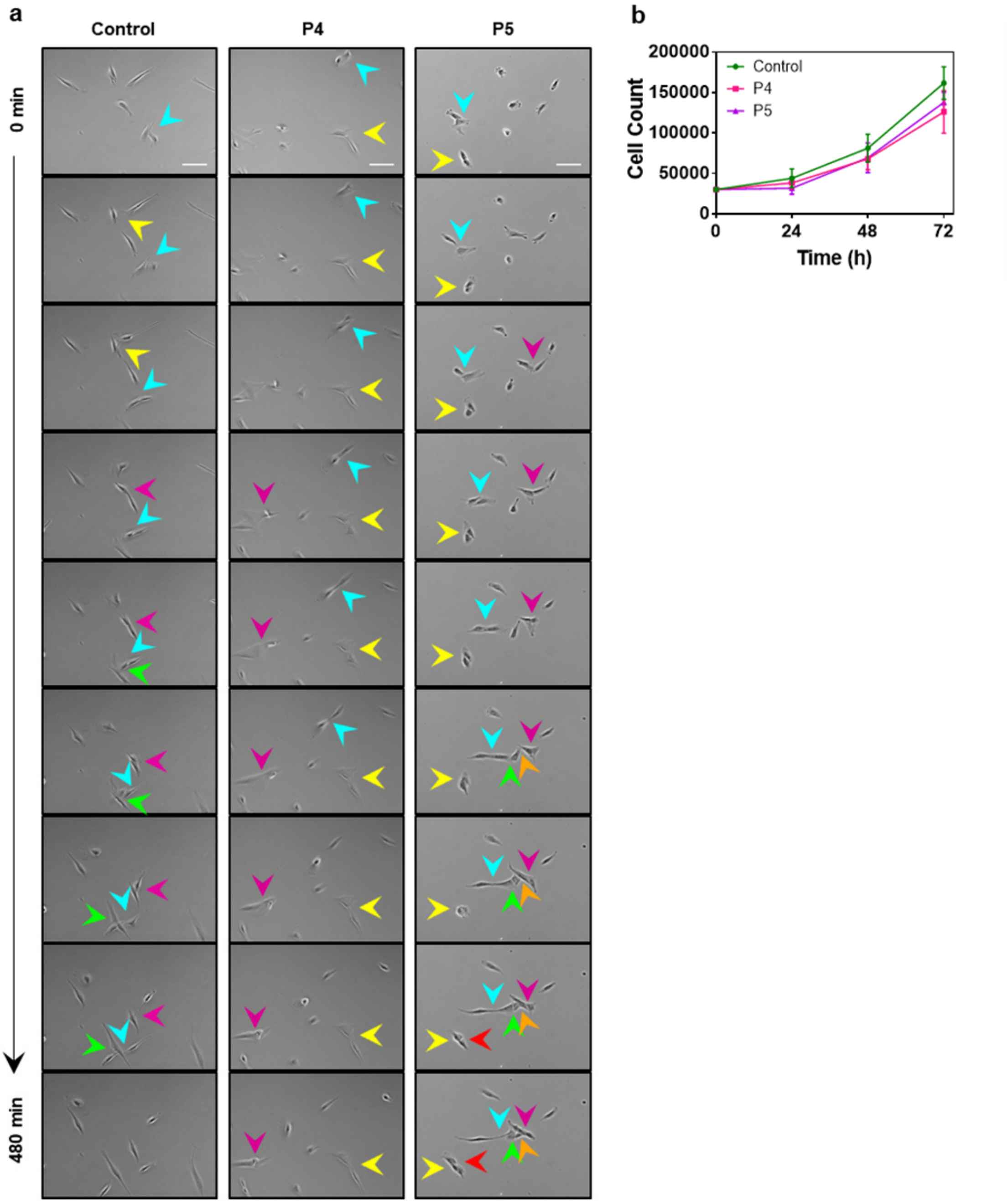

Supplementary Figure 4. Characterization of *ACTB*-AST patient derived primary fibroblasts. (**a**) Representative micrographs of control, patient 4 (P4) and patient 5 (P5) primary fibroblasts at 60 min intervals during 8h migration. Colored markers indicate contacts made between neighboring cells, showing that control cells can migrate past one another, P5 cells aggregate following cell contact and P4 cells are intermediate in their behavior. Scale bars represent 100 µm; (**b**) Growth curve of control (green), P4 (pink) and P5 (purple) primary fibroblasts collected 24 h, 48 h and 72 h after seeding 3x10^4 cells per well (3 experimental repeats with 2 technical replicates each), indicates no significant differences in *ACTB*-AST fibroblast proliferation rate.

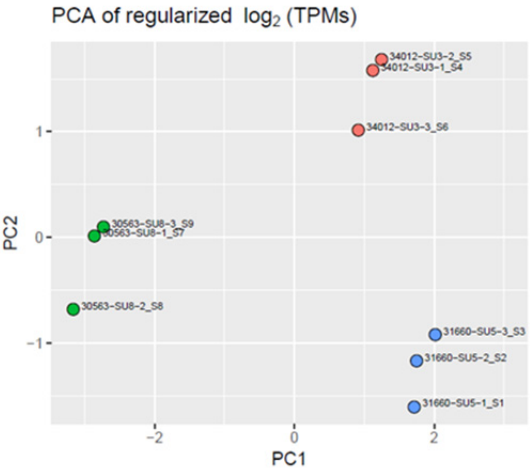

Supplementary Figure 5. Whole-transcriptome analysis of control, P4 and P5 primary dermal fibroblasts. Plot of principal component analysis (PCA) illustrating the grouping of replicates and variation between the different fibroblast cultures. Control fibroblasts (culture ID 31660) are shown in blue, patient 4 fibroblasts (culture ID 34012) are shown in red and patient 5 fibroblasts (culture ID 30563) are shown in green.

a

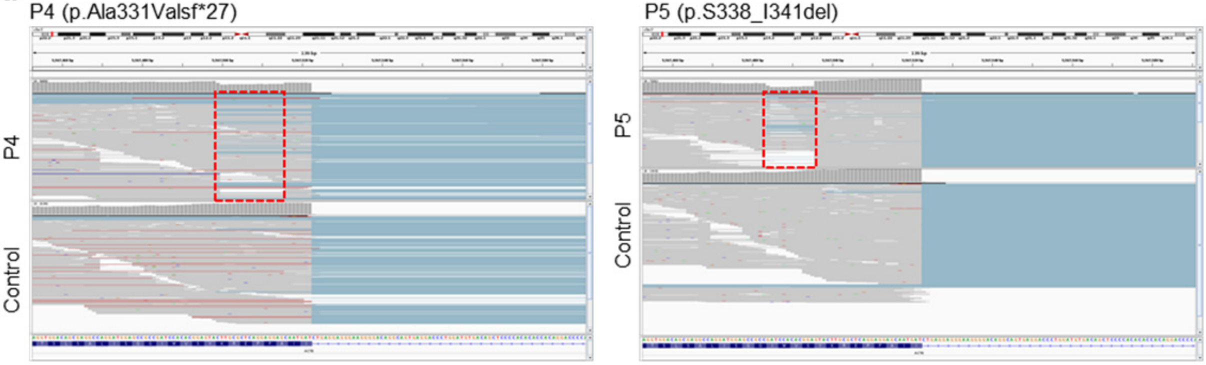

b

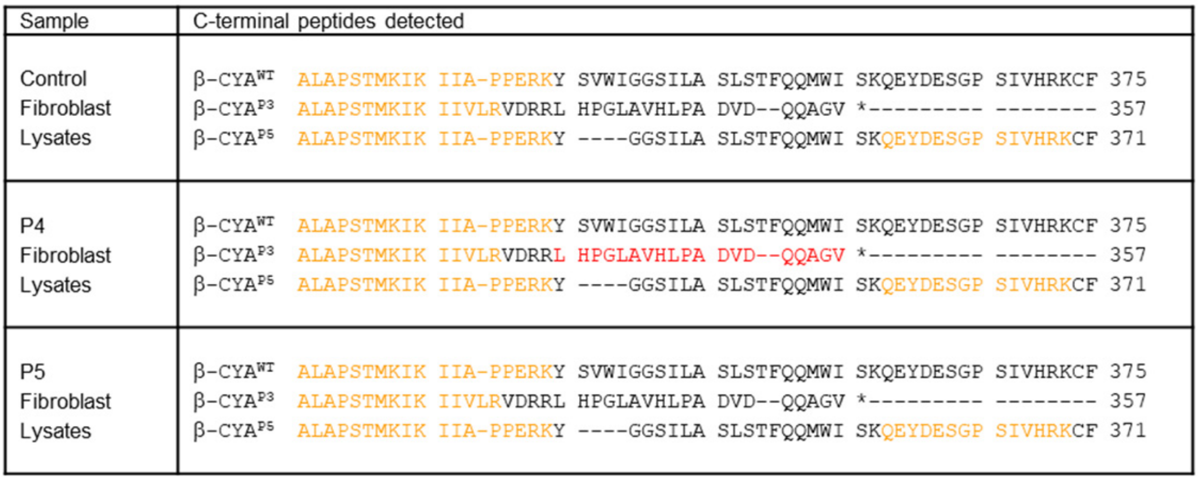

Sample	C-terminal peptides detected
Control Fibroblast Lysates	β-CYA^{WT} ALAPSTMKIK IIA-PPERKY SVWIGGSILA SLSTFQQMWI SKQEYDESGP SIVHRKCF 375 β-CYA^{P3} ALAPSTMKIK IIVLRVDRRL HPGLAVHLPA DVD--QQAGV *--------- -------- 357 β-CYA^{P5} ALAPSTMKIK IIA-PPERKY ----GGSILA SLSTFQQMWI SKQEYDESGP SIVHRKCF 371
P4 Fibroblast Lysates	β-CYA^{WT} ALAPSTMKIK IIA-PPERKY SVWIGGSILA SLSTFQQMWI SKQEYDESGP SIVHRKCF 375 β-CYA^{P3} ALAPSTMKIK IIVLRVDRRL HPGLAVHLPA DVD--QQAGV *--------- -------- 357 β-CYA^{P5} ALAPSTMKIK IIA-PPERKY ----GGSILA SLSTFQQMWI SKQEYDESGP SIVHRKCF 371
P5 Fibroblast Lysates	β-CYA^{WT} ALAPSTMKIK IIA-PPERKY SVWIGGSILA SLSTFQQMWI SKQEYDESGP SIVHRKCF 375 β-CYA^{P3} ALAPSTMKIK IIVLRVDRRL HPGLAVHLPA DVD--QQAGV *--------- -------- 357 β-CYA^{P5} ALAPSTMKIK IIA-PPERKY ----GGSILA SLSTFQQMWI SKQEYDESGP SIVHRKCF 371

Supplementary Figure 6. *ACTB*-AST variant mRNA and protein expression. (**a**) Screenshot of the 'Integrative Genomics Viewer' software interface showing expression of both mutant and native *ACTB* mRNA (red boxed regions) in patient 4 (P4 - p.Ala331Valfs27: 40% reads supporting deletion - reference read count 2413-1798, read count with deletion 1257-2096) and patient 5 (P5 - p.Ser338_Ile341del: 44% reads supporting deletion - reference reads 1877-1943, read count with deletion 1292-1662) fibroblasts, as determined by RNA-Seq; (**b**) LC-MS analysis of control, P4 and P5 primary fibroblast protein samples was performed in the proteomics core facility of Hannover Medical School, as described by Erdmann *et al.*[8]. β-CYA peptides detected by mass spectrometry are shown in color. The peptide unique to the P4 variant is identified only in the P4 sample (red). The peptide region including residues 'SVWI' was not detected in control fibroblasts and accordingly, the 'SVWI' deletion of P5 could not be identified by mass spectrometry.

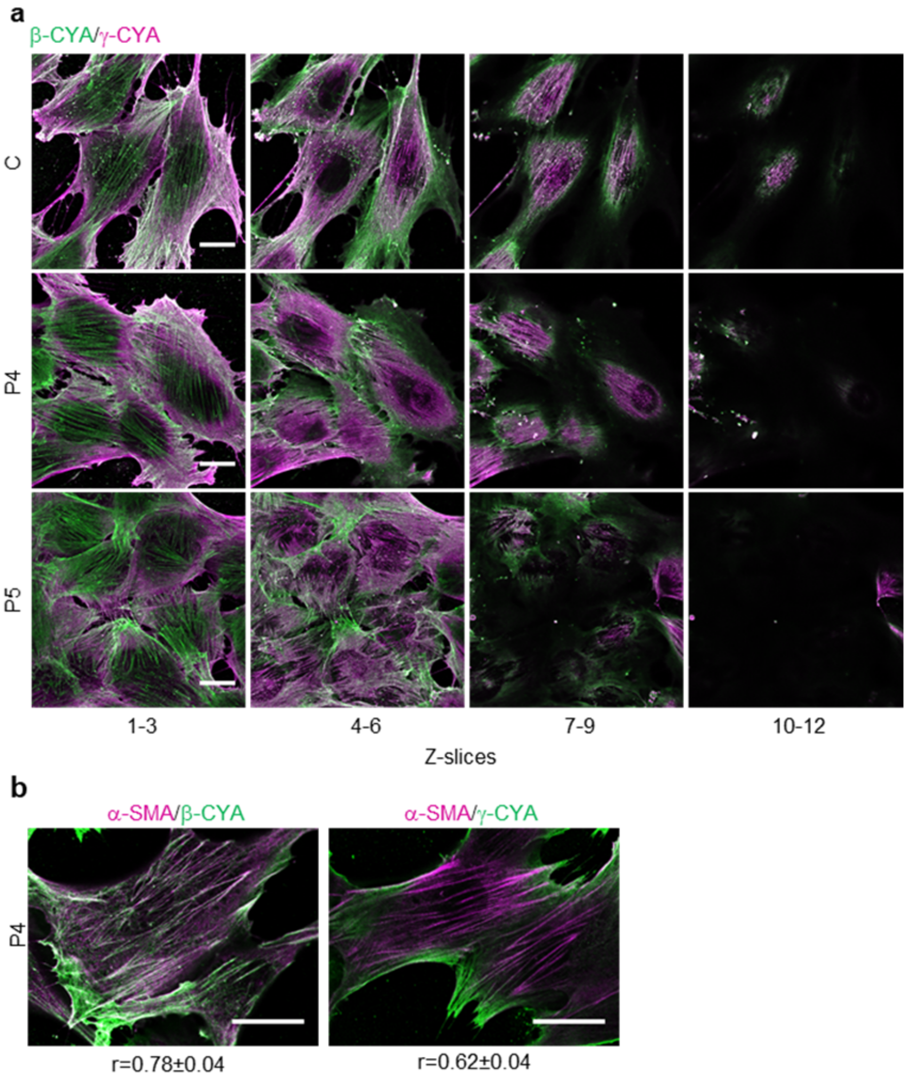

Supplementary Figure 7. Localization of actin isoforms in *ACTB*-AST patient primary fibroblasts. (**a**) Representative images showing β-CYA (green) and γ-CYA (magenta) distribution in control, P4 and P5 fibroblasts. Discrete lateral and axial isoform segregation is consistent with published results[9,10]. Maximum intensity projections for indicated z-stack slices are given. Scale bars represent 15 µm; (**b**) P4 cells co-stained for α-SMA (magenta) with β-CYA (left, green) or γ-CYA (right, green), showing greater overlap of α-SMA with β-CYA within the cells' basal plane, consistent with the findings in P5 cells (see Fig. 4i). The overlap co-efficient (r) is calculated from 28 cells from 3 experiments. Scale bars represent 20 µm.

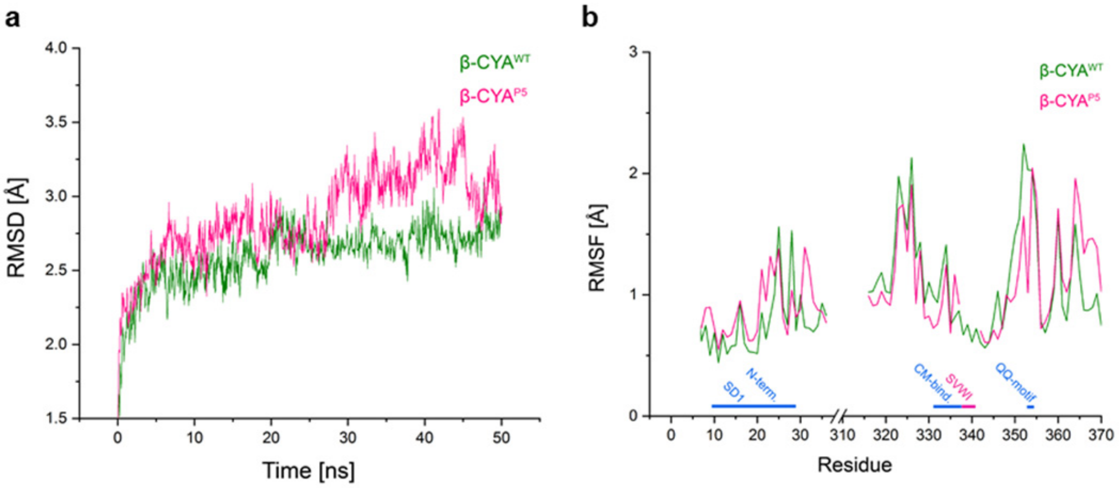

Supplementary Figure 8. Molecular dynamics simulations for β-CYA^{P5} compared to β-CYA^{WT}. (**a**) Comparison of the RMSD plots of the β-CYA^{WT} structure (green) and β-CYA^{P5} model (pink) as a function of MD simulation time. After equilibrium adjustment during the first 20 ns of simulation, the β-CYA^{P5} model shows additional changes in RMSD due to flipping events in different regions of the backbone; (**b**) Comparison of the root mean square fluctuation (*RMSF*) plots of the myosin and α-actinin interacting residues of β-CYA^{WT} (green) and β-CYA^{P5} (pink). Flexible terminal residues were excluded from the representation.

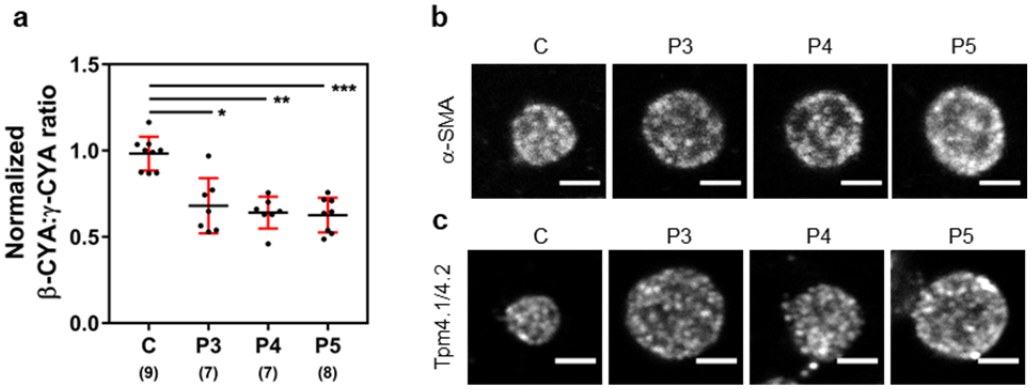

Supplementary Figure 9. Cytoskeletal composition of *ACTB*-AST thrombocytes. (**a**) Immunofluorescence microscopy shows reduced β-CYA:γ-CYA ratios in patient 3 (P3), patient 4 (P4) and patient 5 (P5) thrombocytes compared to those purified from a healthy control (C). The graph shows mean ± s.d., with the number of images analyzed from 1 experiment shown in brackets. Significance was determined with the Kruskal-Wallis test, where * = $p<0.05$, ** = $p<0.01$, *** = $p<0.001$; (**b**) α-SMA was assessed in platelets purified from EDTA-peripheral blood collected from a healthy control (C), P3, P4 and P5. Mid-stack slices show the same regions given in Figure 7a. Representative images show no marked changes in α-SMA localization or intensity between conditions; (**c**) Mid-stack slices of representative platelets from healthy controls and *ACTB*-AST patients show no changes in Tpm4.1/4.2 localization or intensity. All scale bars represent 2 μm.

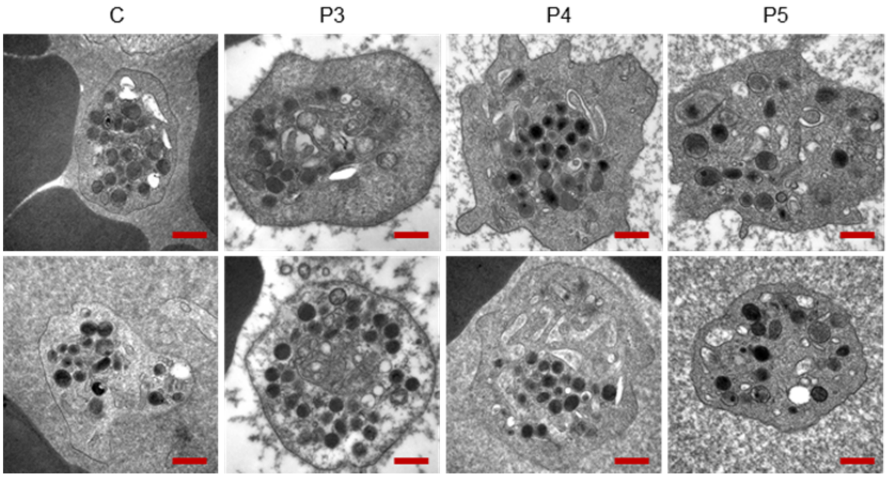

Supplementary Figure 10. Ultrastructural assessment of control and *ACTB*-AST patient platelets. Platelets in EDTA-peripheral blood from a healthy control (C), patient 3 (P3), patient 4 (P4), and patient 5 (P5) were analyzed by transmission electron microscopy. Images reveal regular intracellular content (dense granules, α-granules, mitochondria and lysosomes) in both healthy control and *ACTB*-AST patient samples. All scale bars represent 0.5 µm.

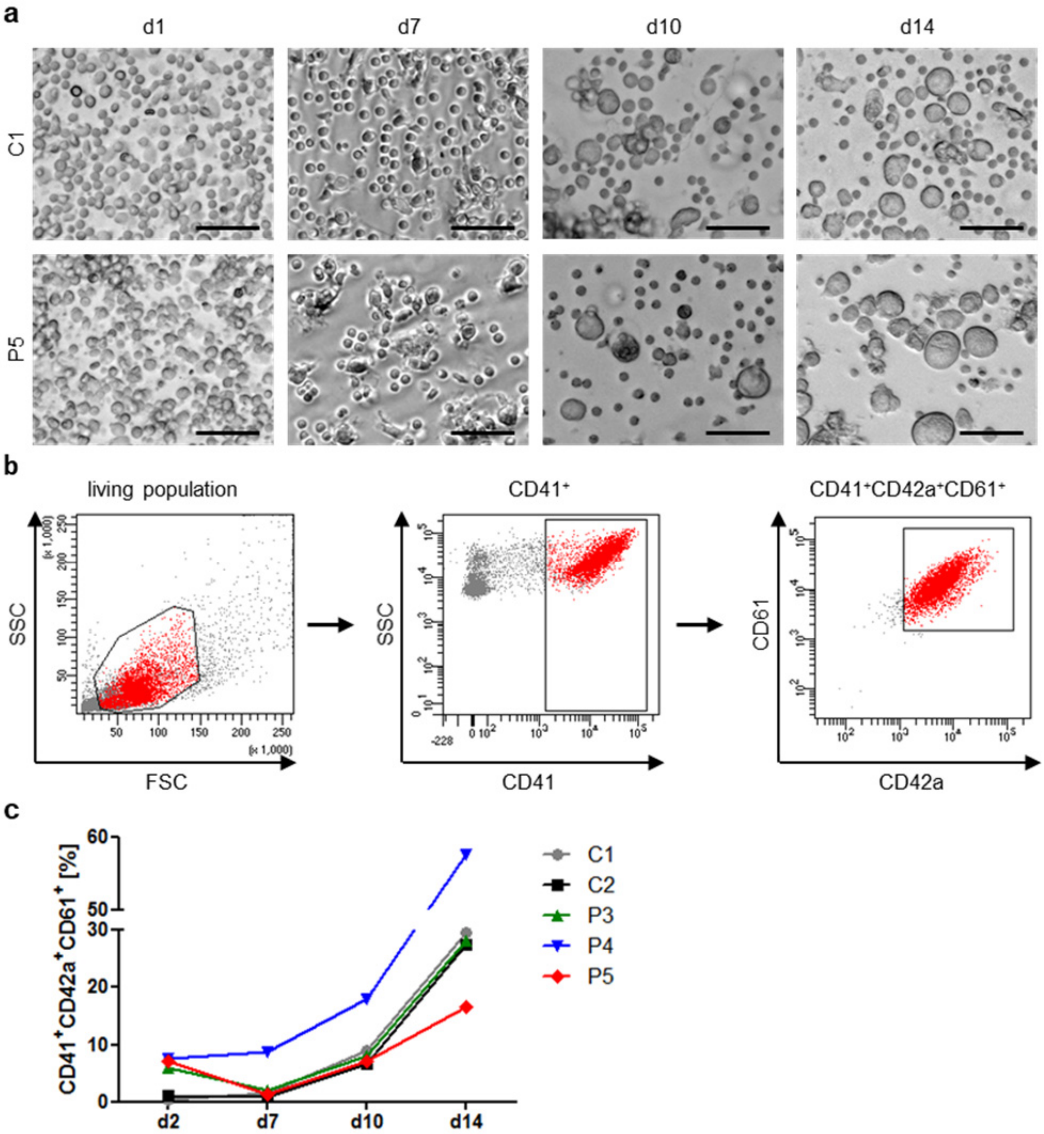

Supplementary Figure 11. Differentiation of MKs from healthy donors and *ACTB-AST* patients. (**a-b**) MKs differentiated from PBMCs isolated from whole blood samples (n=1); (**a**) Morphology of control (top row) and patient 5 (P5, bottom row) cells on days (d) 1, 7, 10 and 14 of megakaryocyte differentiation. Images show enlarged cells phenotypic of MKs on d10 and d14. All scale bars represent 50 µm; (**b**) Example of the flow cytometry gating strategy used to identify CD41, CD42a and CD61 triple positive MKs. Data show P3 on day 14 of differentiation; (**c**) Content of $CD41^+CD42a^+CD61^+$ cells, analyzed by flow cytometry throughout the differentiation of PBMCs to MKs of two healthy controls (black and grey), P3 (green), P4 (blue), and P5 (red).

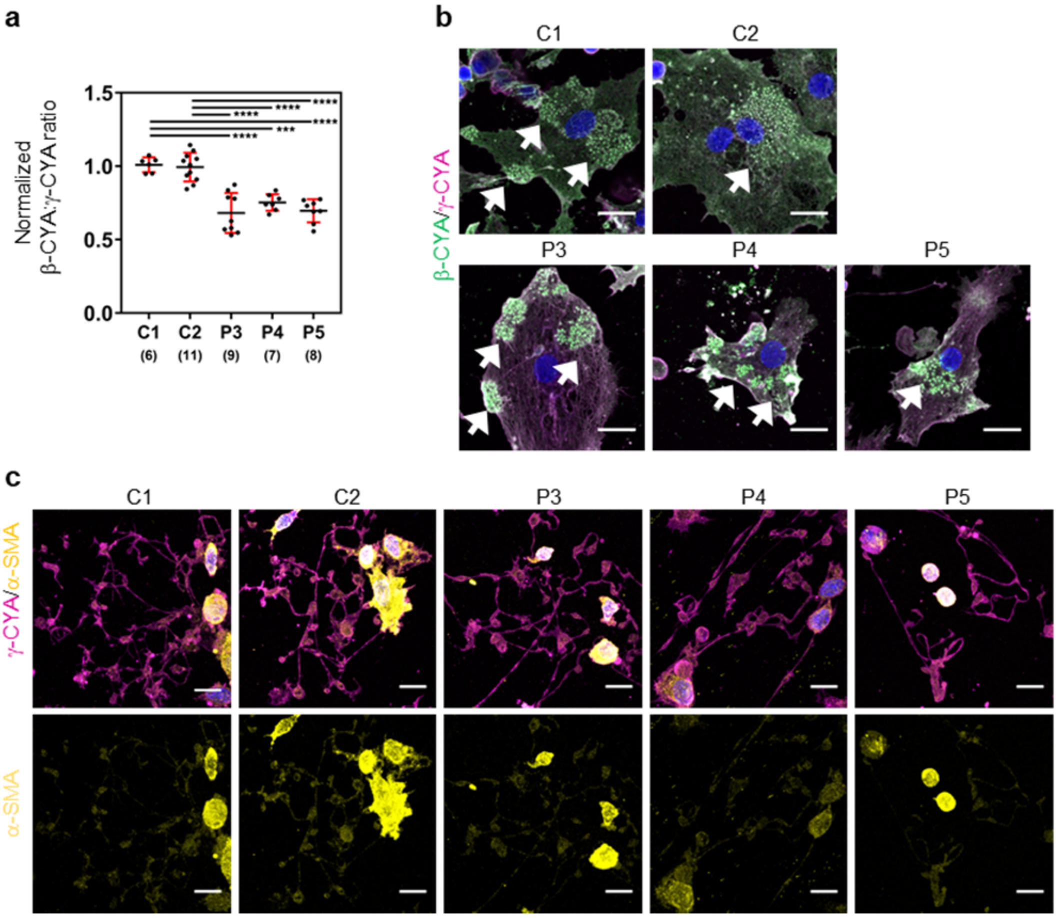

Supplementary Figure 12. Actin isoforms in healthy control and *ACTB*-AST megakaryocytes. (**a**) Immunofluorescence microscopy shows reduced β-CYA:γ-CYA ratios in patient 3 (P3), patient 4 (P4) and patient 5 (P5) MKs compared to two healthy controls (C1 and C2). Data show mean ± s.d., with the number of images analyzed from 1 experiment indicated in brackets. Significance was determined with a one-way ANOVA, where *** = $p<0.001$, **** = $p<0.0001$; (**b**) β-CYA (green) and γ-CYA (magenta) distribution in podosome-forming cells differentiated from C1, C2, P3, P4 and P5 PBMCs. Representative maximum intensity projections demonstrate the incorporation of β-CYA in podosomes (white arrows) in both healthy controls and *ACTB*-AST patient cells. Scale bars represent 15 µm; (**c**) γ-CYA (magenta) and α-SMA (yellow) distribution were assessed in proplatelet-producing MKs differentiated from C1, C2, P3, P4 and P5 PBMCs. Maximum intensity projections show that α-SMA expression and localization are unchanged between control and patient MK. Images correspond to those shown in Figure 8a. Scale bars represent 10 µm.

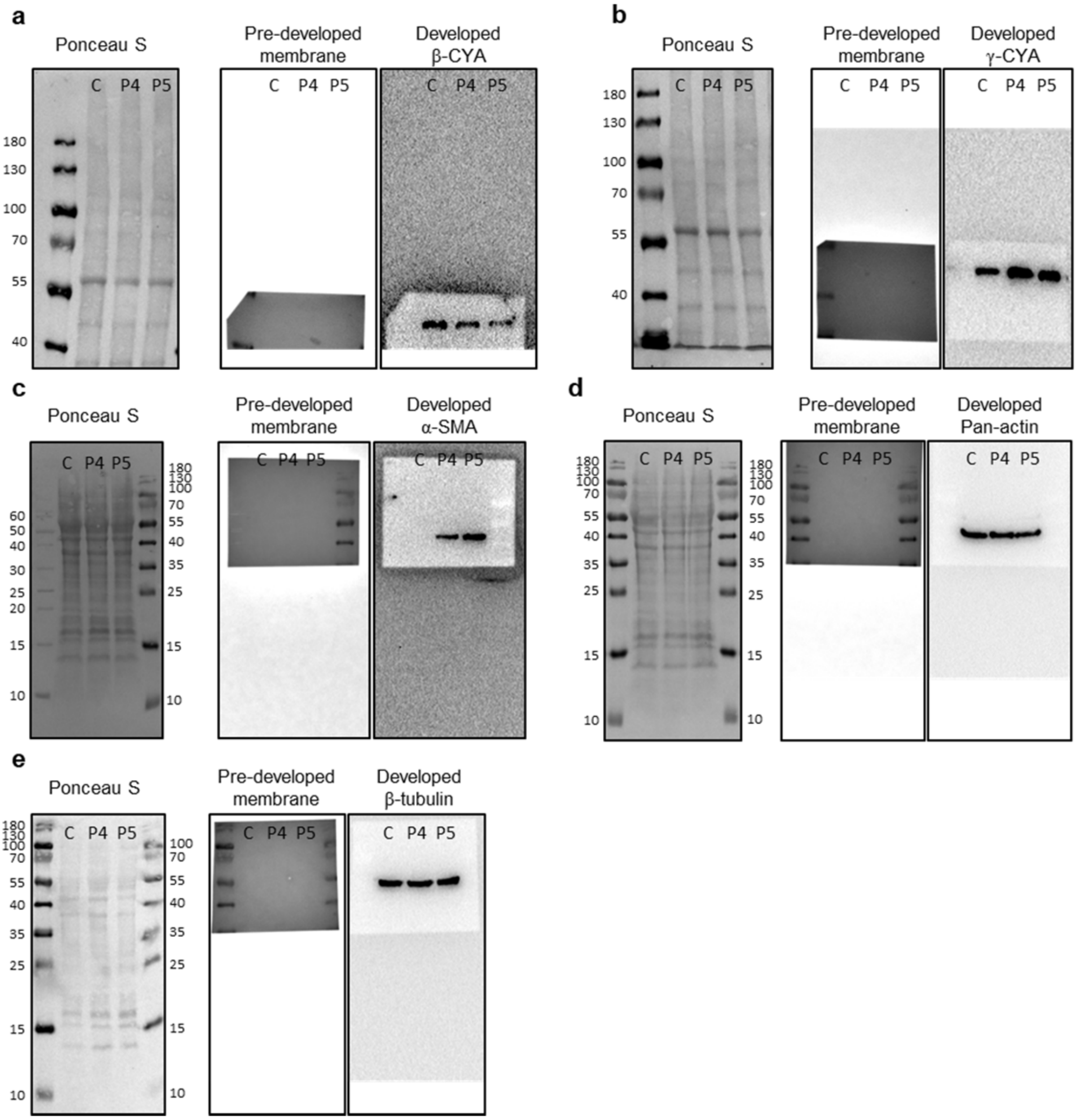

Supplementary Figure 13. Western blots of actin isoforms in *ACTB*-AST fibroblasts. Protein lysates from control (C), Patient 4 (P4) and Patient 5 (P5) fibroblasts were separated by SDS-PAGE and blotted onto nitrocellulose membrane to visualize expression levels of (**a**) β-CYA, (**b**) γ-CYA, (**c**) α-SMA, (**d**) total actin and (**e**) β-tubulin (loading control). Following Ponceau S staining (left in each sub-panel) and blocking, membranes were cut into 2-4 segments and probed for proteins within different size ranges. Pre-stained markers were visualized on the pre-developed membrane (mid in each sub-panel) prior to chemiluminescent membrane development (right in each sub-panel). Subpanels a, b, d and e are representative of 9-10 technical replicates from 6 lysates, whilst c is representative of 3 technical replicates from 3 lysates. Molecular weights indicated are in kDa.

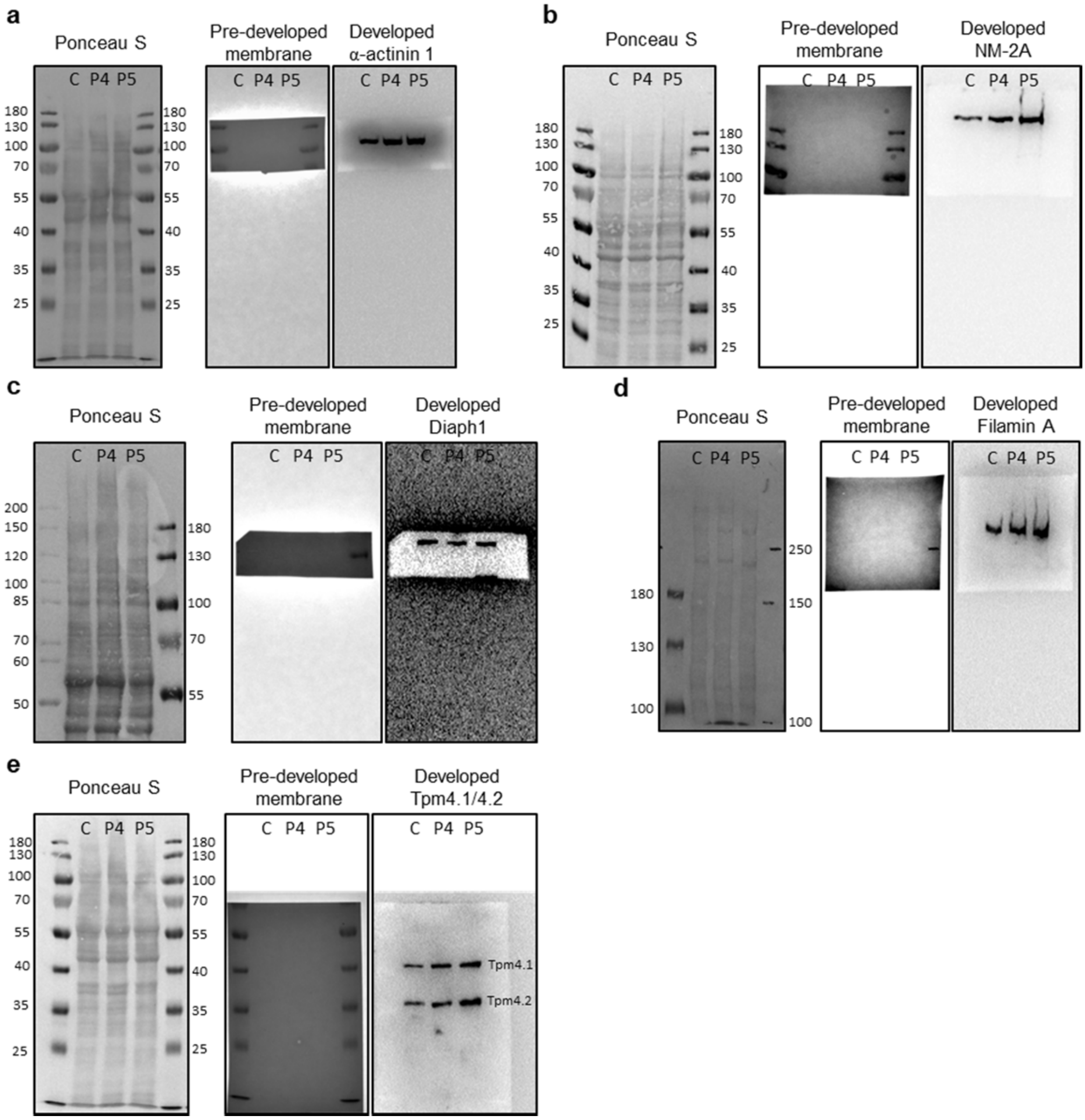

Supplementary Figure 14. Western blots of candidate actin binding proteins in *ACTB*-AST fibroblasts. Protein lysates from control (C), Patient 4 (P4) and Patient 5 (P5) cells were separated by SDS-PAGE and blotted onto nitrocellulose membrane to visualize (**a**) α-actinin 1, (**b**) NM-2A, (**c**) Diaph1, (**d**) Filamin A and (**e**) Tpm4.1/4.2 expression. Following Ponceau S staining (left in each) and blocking, cut membranes were probed for different sized proteins. Pre-stained markers were visualized on the pre-developed membrane (mid in each) prior to chemiluminescent membrane development (right in each). Images shown are representative of 6 technical replicates from 3 lysates. Molecular weights indicated are in kDa.

Supplementary Table 1. ***ACTB*** **missense and loss of function variants in the 3' region listed in the gnomAD database (canonical transcript ENST00000331789)**

Genomic position GRCh37 (hg19) NC_000007.13	Nucleotide substitution	Amino acid change	Allele count	Allele number	Allele frequency	Zygocity
5567393	G / A	Arg372Cys	1	246238	0.000004061	het
5567414	A / T	Ser365Thr	1	246234	0.000004061	het
5567417	C / G	Glu364Gln	1	246226	0.000004061	het
5567450	GGAAGGTGGACAGC / G	Leu349SerfsTer29	1	246194	0.000004062	het
5567459	A / T	Ser350Thr	1	246180	0.000004062	het
5567500	T / C	Lys336Arg	1	30920	0.00003234	het
5567664	C / A	Ala319Ser	1	246268	0.000004061	het

Supplementary Table 2. List of antibodies used in this study

Primary Antibodies						
Target	**Specificity**	**Origin**	**Product #**	**Dilution Factors**		
				IFM	**WB**	**FCM**
β-CYA	Mouse monoclonal IgG$_1$	Prof C. Chaponnier	-	1:50	1:500	-
	Clone 4C2	Available at AbD Serotec, EMD Millipore and Nordic-Mubio				
		Dugina *et al.* 2009, *J Cell Sci*				
γ-CYA	Mouse monoclonal IgG$_{2b}$	Prof C. Chaponnier	-	1:100	1:5000	-
	Clone 2A3	Available at AbD Serotec, EMD Millipore and Nordic-Mubio				
		Dugina *et al.* 2009, *J Cell Sci*				
α-SMA	Mouse monoclonal IgG$_{2a}$	Prof C. Chaponnier	-	1:50	1:500	-
	Clone 1A4	Available at Abcam, EMD Millipore, Sigma Aldrich, etc.				
		Skali *et al.* 1986, *J Cell Biol*				
γ-SMA	Mouse monoclonal IgG$_1$	Prof C. Chaponnier;	-	1:50	1:100	-
	Clone 20D2	Arnoldi *et al.* 2012, Eur J Cell Biol				
Pan-actin	Rabbit polyclonal	Cell Signaling Technology	4968S	-	1:1000	-
β-tubulin	Mouse monoclonal IgG$_1$ Clone DM1B	Santa Cruz	sc-58880	1:50	1:200	-
NM-2A	Rabbit polyclonal	Covance	PRB-440P	1:500	1:1000	-
Filamin A (N-term)	Mouse monoclonal IgG$_{2a}$ Clone E-3	Santa Cruz	sc-17749	1:100	-	-
Filamin A (C-term)	Rabbit monoclonal Clone EP2405Y	Abcam	Ab76289	1:100	1:10000	-
α-actinin 1	Rabbit polyclonal	Thermo Scientific	PA5-17308	-	1:1000	-
α-actinin 1	Mouse monoclonal IgG$_1$ Clone AT6/172	Merck Millipore	MAB1682	1:100	-	-
Tpm4	Rabbit polyclonal	Merck Millipore	AB5449	1:500	1:1000	-
Diaph1	Rabbit polyclonal	Abcam	Ab96784	1:100	1:500	-
CD61-AlexaFluor 647	Mouse monoclonal IgG$_1$ Clone VI-PL2	Biolegend	336408	1:25	-	-
CD42a-PE	Mouse monoclonal IgG$_1$ Clone ALMA.16	BD Biosciences	558819	-	-	As per manufacturer
CD41-APC/CY7	Mouse monoclonal IgG$_1$ Clone HIP8	Biolegend	303716	-	-	As per manufacturer
CD61-APC	Mouse monoclonal IgG$_1$ Clone VI-PL2	Biolegend	336412	-	-	As per manufacturer

Secondary Antibodies							
Host/Target	**Isotype**	**Conjugate**	**Company**	**Product #**	**Dilution Factor**		
					IFM	**WB**	**FCM**
Goat anti Mouse	IgG$_1$	AlexaFluor 488	Jackson Immunoresearch	115-545-205	1:400	-	-
Goat anti Mouse	IgG$_{2a}$	Rhodamine	Jackson Immunoresearch	115-295-206	1:100	-	-
Goat anti Mouse	IgG$_{2b}$	CY5	Jackson Immunoresearch	115-175-207	1:100	-	-
Goat anti Mouse	IgG	AlexaFluor 488	Jackson Immunoresearch	115-545-146	1:400	-	-
Goat anti Mouse	IgG	CY5	Jackson Immunoresearch	115-175-146	1:100	-	-
Goat anti Rabbit	-	AlexaFluor 488	Jackson Immunoresearch	111-545-144	1:200	-	-
Goat anti Rabbit	-	CY3	Jackson Immunoresearch	111-165-144	1:100	-	-
Goat anti Mouse	-	HRP	Thermo Scientific	32430	-	1:1000	-
Goat anti Rabbit	-	HRP	Thermo Scientific	32460	-	1:1000	-

Supplementary References

1. von der Ecken, J., Heissler, S.M., Pathan-Chhatbar, S., Manstein, D.J. & Raunser, S. Cryo-EM structure of a human cytoplasmic actomyosin complex at near-atomic resolution. *Nature* **534**, 724-8 (2016).
2. Furch, M., Remmel, B., Geeves, M.A. & Manstein, D.J. Stabilization of the actomyosin complex by negative charges on myosin. *Biochemistry* **39**, 11602-8 (2000).
3. Varkuti, B.H. *et al.* A novel actin binding site of myosin required for effective muscle contraction. *Nat Struct Mol Biol* **19**, 299-306 (2012).
4. Galkin, V.E., Orlova, A., Salmazo, A., Djinovic-Carugo, K. & Egelman, E.H. Opening of tandem calponin homology domains regulates their affinity for F-actin. *Nat Struct Mol Biol* **17**, 614-6 (2010).
5. Pertuy, F. *et al.* Myosin IIA is critical for organelle distribution and F-actin organization in megakaryocytes and platelets. *Blood* **123**, 1261-9 (2014).
6. Bender, M. *et al.* ADF/n-cofilin-dependent actin turnover determines platelet formation and sizing. *Blood* **116**, 1767-75 (2010).
7. Lek, M. *et al.* Analysis of protein-coding genetic variation in 60,706 humans. *Nature* **536**, 285-91 (2016).
8. Erdmann, J. *et al.* Glucosyltransferase-dependent and -independent effects of TcdB on the proteome of HEp-2 cells. *Proteomics* **17**, 10.1002/pmic.201600435 (2017).
9. Dugina, V., Zwaenepoel, I., Gabbiani, G., Clement, S. & Chaponnier, C. Beta- and gamma-cytoplasmic actins display distinct distribution and functional diversity. *J Cell Sci* **122**, 2980-2988 (2009).
10. Latham, S.L. *et al.* Cooperation between beta- and gamma-cytoplasmic actins in the mechanical regulation of endothelial microparticle formation. *FASEB J* **27**, 672-83 (2013).